

Pseudo-Chaotic Time Hopping For UWB Impulse Radio

Gian Mario Maggio, *Member, IEEE*, Nikolai Rulkov, and Luca Reggiani, *Student Member, IEEE*

Abstract—In this paper, we propose a pseudo-chaotic modulation suitable for ultrawide-bandwidth impulse-radio communication systems. The coding scheme is based upon controlling the symbolic dynamics of a chaotic map for encoding the digital information to be transmitted. The pseudo-chaotic time hopping enhances the spread-spectrum characteristics of the system, by removing most periodic components from the transmitted signal. A maximum-likelihood detector for the proposed scheme is presented and its scalability features are illustrated. Finally, theoretical performance bounds for both soft and hard Viterbi decoding are derived and compared with the simulation results.

Index Terms—Chaos, impulse radio, maximum-likelihood detection, performance bounds, scalability, symbolic dynamics, UWB.

I. INTRODUCTION

IN THE LAST few years, there has been a rapidly growing interest toward ultrawide-bandwidth (UWB) impulse-radio (IR) communication systems. These systems make use of ultrashort duration (<1 ns) pulses which yield ultra-wide bandwidth signals characterized by extremely low power spectral densities [1], [2]. UWB-IR systems are particularly promising for short-range wireless communications as they combine reduced complexity with low power consumption, low probability of intercept (LPI), immunity to multipath fading, and multiuser capabilities [3]. Current UWB-IR communication systems typically employ pseudo-random noise (PN) coding for channelization purposes and pulse-position modulation (PPM) for encoding the binary information.

In [4] it was first proposed the use of aperiodic sequences of pulses in the context of chaos-based communication system. A few schemes with chaotic modulation of the inter-pulse intervals were then proposed and studied in [5], [6]. In particular, the scheme presented in [5] is based on the self-synchronizing properties of chaotic systems. In this system, the information is modulated into pulse trains by introducing time dithering and

retrieved coherently at the receiver by means of chaotic synchronization of the pulse trains. In [7] a similar scheme was designed for the transmission of binary information and named chaotic pulse-position modulation (CPPM). Recently, a scheme introducing a frequency modulation on top of the chaotic time hopping has been proposed in [8].

We emphasize that the use of nonperiodic (chaotic) codes enhances the spread-spectrum characteristics of the system by removing the spectral features of the signal transmitted, thus resulting in a low probability of intercept. In addition, the absence of spectral lines may translate into a reduced interference toward other services such as the GPS (global positioning system) [9].

In this work, we propose a pseudo-chaotic (PC) modulation code suitable for UWB-IR systems. The proposed scheme, that we call pseudo-chaotic time hopping (PCTH), exploits the symbolic dynamics of a chaotic map at the transmitter in order to encode the binary information [10]. The basic idea underlying PCTH is somehow related to the one suggested by Hayes *et al.* in [11], and further developed by Schweizer *et al.* [12]. Namely, it consists of controlling the dynamics of a chaotic system in order to obtain the desired symbolic sequence [13].

From the viewpoint of communication theory, the PCTH scheme should be considered in the context of spread-spectrum (SS) communications, which includes UWB impulse radio. The PCTH scheme combines pseudo-chaotic encoding with a multilevel PPM. The pseudo-chaotic encoder performs a spreading and acts as a form of convolutional coding [14]. The request for spreading, though, results in a large number of levels in the transmitter. This in general would require, at the receiver side, a convolutional decoder with a large number of states. By exploiting concepts from symbolic dynamics we show that the PCTH signal can be decoded with a Viterbi detector [16] of reduced complexity, i.e., with a limited number of states. Moreover, detectors of different complexity (and performance) may coexist while decoding the same transmitted PCTH signal. We emphasize that this scalability property, which is not present in conventional convolutional coding, adds flexibility in terms of the receiver design.

The paper is organized as follows. In Section II, we illustrate the theory underlying the PCTH scheme. Namely, Section II.B deals with the symbolic dynamics of chaotic maps. The structure of the pseudo-chaotic encoder is discussed in detail in Section III. Section IV is concerned with the nature of the PCTH signal and in particular with its spectrum (see Section IV.D). Then, in Section V we discuss different possible implementations of the PCTH decoder with special emphasis on maximum-likelihood (ML) detection and the scalability of the receiver. Finally, Section VI reports about the performance of

Manuscript received March 8, 2001; revised August 9, 2001. The work of G.M. Maggio and N. Rulkov was supported in part by the Army Research Office under Grant DAAG55-98-1-0269 and in part by the U.S. Department of Energy, Office of Basic Energy Sciences, under Grant DE-FG03-90ER14138. This paper was recommended by Guest Editor M Ogorzalek.

G. M. Maggio is with the Center for Wireless Communications, University of California at San Diego, La Jolla, CA 92093-0407 USA, and also with STMicroelectronics, Inc., AST-San Diego, CA 92121 USA (e-mail: gmaggio@ucsd.edu; gian-mario.maggio@st.com).

N. Rulkov is with the Institute for Nonlinear Science (INLS), University of California at San Diego, La Jolla, CA 92093-0402 USA (e-mail: nrulkov@ucsd.edu).

L. Reggiani is with the Dipartimento di Elettronica ed Informazione, Politecnico di Milano, Milan 20133, Italy (e-mail: reggiani@elet.polimi.it).

Publisher Item Identifier S 1057-7122(01)10384-3.

the PCTH scheme in the presence of noise. In particular, theoretical performance bounds are derived and compared with the simulation results.

II. PCTH: THEORY

In this section, we illustrate the theory behind the PCTH scheme. To this aim, we start by recalling some useful concepts about the shift map and its symbolic dynamics.

A. Shift Map and Bernoulli Shift

The shift map is perhaps the simplest example of chaotic system and it possesses all the peculiar features of chaotic dynamics [17]. Let's indicate by Σ_2 the symbol space of binary "0"s and "1"s, that is $\Sigma_2 = \{(s_0 s_1 s_2 \dots) | s_i = 0 \text{ or } s_i = 1\}$. Then, the *shift map* $\sigma : \Sigma_2 \rightarrow \Sigma_2$ is defined as [17]

$$\sigma(s_0 s_1 s_2 \dots) = s_1 s_2 s_3 \dots \quad (1)$$

that is, it simply "forgets" the first entry in a sequence, and shifts all other entries one position to the left.

An equivalent way of studying the shift map is to represent the state x of the corresponding discrete (one-dimensional) dynamical system as a binary expansion

$$x = 0.b_1 b_2 b_3 \dots \equiv \sum_{j=1}^{\infty} 2^{-j} b_j \quad (2)$$

where each of the bits b_j is either a "0" or a "1", and $x \in I = [0, 1]$. Then, the effect of the shift map applied to the binary sequence $\{b_j\}_{j=1}^{\infty}$ is described by the *Bernoulli shift map* [15]

$$x_{k+1} = 2x_k \bmod 1 \quad (3)$$

whose graph is shown in Fig. 1. Referring to (3), the successive iterates of x are obtained by moving the separating point one position to the right (multiplication by 2) and setting to zero the first integer digit (modulo operation) [18]. Hence, digits which are initially far to the right of the separating point, thus having only a very slight influence on the value of x , eventually become the first fractional digit.

B. Symbolic Dynamics

Symbolic dynamics may be defined as a "coarse-grained" description of the evolution of a dynamical system [13]. The idea is to partition the state space and to associate a symbol to each partition. Then, a trajectory of the dynamical system can be analyzed as a symbolic sequence. From this perspective, a chaotic system may be seen as a natural information source [20]. We illustrate these concepts in the case of the Bernoulli shift map, shown in Fig. 1. In this case, the state space is represented by the invariant interval $I = [0, 1]$. In order to ensure that the symbolic dynamics give rise to a topological Markov chain a so-called *Markov partition* has to be selected [21]. A map admitting a Markov partition is also said a *Markov map*. These properties will turn out to be especially useful in Section V.C.

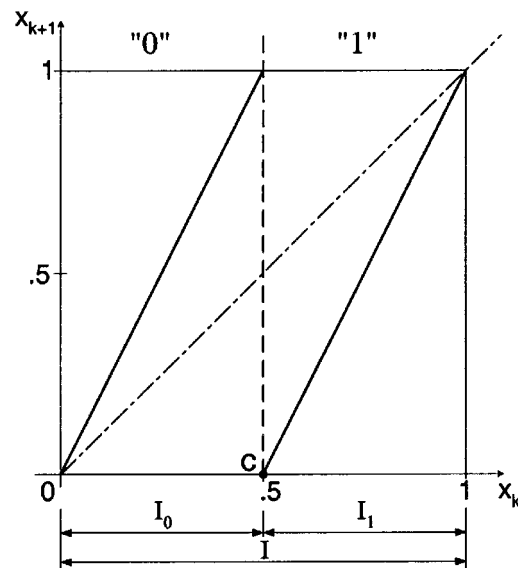


Fig. 1. The Bernoulli shift map with the definition of the symbolic dynamics used in the PCTH scheme. The invariant interval $I = [0, 1]$ is partitioned with respect to the critical point $c = 0.5$. The subintervals I_0 and I_1 are assigned the binary symbols "0" and "1", respectively.

In the case of the Bernoulli shift map we select a Markov partition by splitting the interval $I = [0, 1]$ with respect to the critical point $c = 0.5$ and, correspondingly, we define the two subintervals $I_0 = [0, 0.5)$ and $I_1 = [0.5, 1]$, as shown in Fig. 1. In order to obtain a symbolic description of the dynamics of the chaotic map under consideration we associate the binary symbol "0" and "1" to the subintervals I_0 and I_1 , respectively. Then, the evolution of the Bernoulli map can be characterized in terms of a symbolic sequence $\mathcal{S} = \{010010\dots\}$ [22].

III. PSEUDO-CHAOTIC ENCODER

The basic block around which the pseudo-chaotic encoder is built is an implementation of the Bernoulli shift map (Section III.A). An interpretation of its operation the context of control and information theory is given in Section III.B and Section III.C, respectively.

A. Implementation of the Bernoulli Shift

In this work, the Bernoulli shift process is approximated by means of a finite-length shift register R . The shift operation corresponds to a multiplication by a factor 2, while the modulo 1 operation is realized by discarding the MSB at each step (see Section II.A).

In the scheme of Fig. 2 the shift register R is fed with the binary information $c(k)$ to be transmitted. In particular, at each step (or clock impulse) the most recent bit of information is assigned the least-significant bit (LSB) position in the shift register while the old most-significant bit (MSB) is discarded. The situation is depicted in Fig. 3(a). We assume the binary stream $c(k)$ feeding the shift register to be an i.i.d. (independent and identically distributed) sequence. In practice this may be achieved by inserting a data compression and (if necessary) a data scrambling block in front of the shift register R , as shown schematically in Fig. 2.

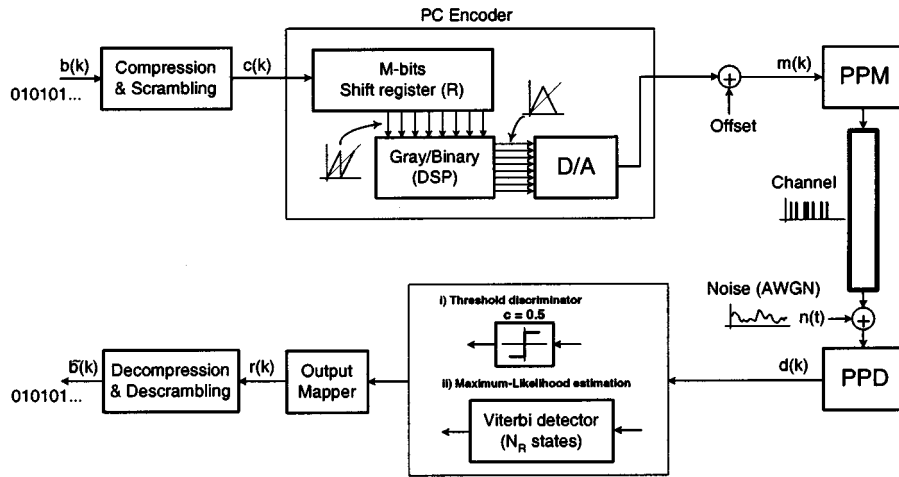


Fig. 2. Simplified block diagram of the PCTH scheme. The encoder is characterized by $N = 2^M$ levels, where M is the number of bits in the shift register R . In general, the receiver can be realized with $N_R \leq N$ states, as discussed in Section V.D.

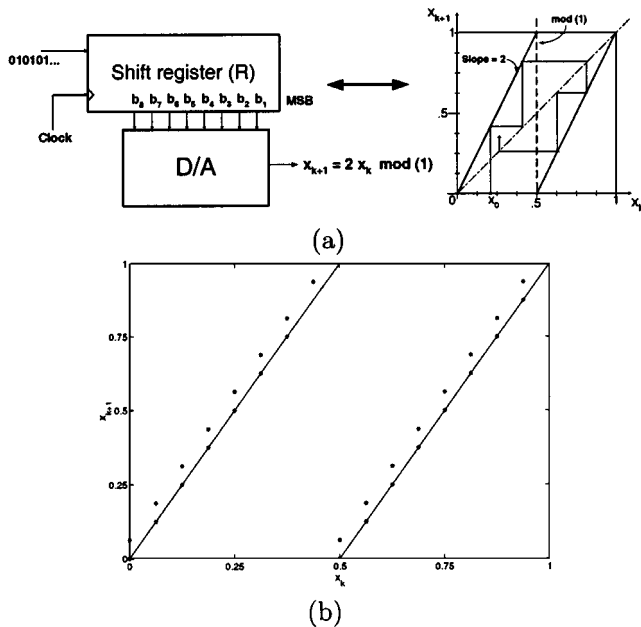


Fig. 3. (a) Implementation of the Bernoulli shift map by means of a M -bit shift register R (and a D/A converter). (b) Effect of the state quantization (for $M = 4$).

Due to the finite length of the shift register R , the dynamics of the Bernoulli shift can only be approximated, as the admissible states assume discrete values. Namely, by considering an M -bit shift register, the generic state x can be expressed as

$$x = 0.b_1b_2 \dots b_M \equiv \sum_{j=1}^M 2^{-j} b_j \quad (4)$$

where b_1 and b_M represent the MSB and the LSB, respectively. In particular, for a M -bit shift register the quantization error ε is bounded from above by [18]

$$\varepsilon(M) < 2^{-M}$$

which tends to zero for $M \rightarrow \infty$. The effect of the state quantization on the Bernoulli shift map is illustrated in Fig. 3(b), for the case $M = 4$.

B. Pseudo-Chaotic Encoding as Control of Chaos

The pseudo-chaotic encoding acts as a form of predictive control with respect to the symbolic dynamics of the Bernoulli shift equation (3), according to the state definition equation (4). In fact, the symbolic dynamics of the Bernoulli shift (with the partition introduced in Section II.B) are determined solely by the successive values of the MSB in the shift register R . Referring to (4), it is clear that the first bit on the right of the separating point determines whether the iterate falls within I_0 or I_1 , the remaining bits deciding only the relative position within I_j , with $j = 0, 1$. But the value of the MSB at step k coincides with the value of the LSB, M steps before, at step $(k - M)$. In turn, the LSB contains the current bit of information $c(k)$. In this sense, the PC encoding is predictive in its nature.

Similar forms of control of the symbolic dynamics of chaotic oscillators, with the purpose of transmitting digital information, have been proposed in the past by Hayes *et al.* in [11] and by Schweizer *et al.* [12]. The underlying idea was to exploit the sensitivity to initial conditions of a chaotic system for controlling its symbolic dynamics by means of only small external perturbations. If properly applied, the small control action would induce the chaotic system (typically a chaotic oscillator) to follow the desired symbolic sequence. Recently, the performance of this kind of systems in the presence of noise and distortion in the channel has been evaluated by Williams [23].

In the proposed pseudo-chaotic encoder the control problem is solved *a priori* by direct “synthesis” of the chaotic signal, starting from the binary information to be transmitted. In this way, the control apparatus becomes significantly simpler than in [11], [12], and its resolution can be increased arbitrarily by simply increasing the length M of the shift register R . From this perspective, the injection of a new bit of information in the LSB of the shift register may be interpreted as a perturbation of the state of the dynamical system, in order to make it following the desired symbolic sequence.

C. Pseudo-Chaotic Encoding as Convolutional Coding

From the viewpoint of information theory, the shift register structure implementing the Bernoulli shift may be seen as a form of convolutional coding [24]. The memory of the structure is represented by the shift register which stores the last M input bits. Each input bit causes an output of M bits; thus, the overall rate is $1/M$.

In the case of the Bernoulli shift map the output of the encoder coincides with the shift register content at the next encoding step. In general, though, the shift register may be followed by a digital processing unit, as discussed in Section III.D. Moreover, it is clear that the encoded signal can be recovered by a Viterbi detector (VD), that performs a ML decoding when the noise is additive white Gaussian noise (AWGN).

D. Map Transformation

In general, the shift register implementing the Bernoulli shift map may be followed by a digital signal processing (DSP) unit for generating more complex chaotic maps, as illustrated in Fig. 2. This can be useful for spectral shaping purposes (see Section IV.D and/or for enhancing the ML detection, as discussed in Section V.C).

In this work we consider the simple transformation of the Bernoulli shift map (3) into the *tent map*, described by

$$x_{k+1} = 1 - 2|x_k - 0.5|. \quad (5)$$

This is done in order to achieve a greater robustness of the system in the presence of noise by avoiding (zero-order) discontinuities in the map. Such transformation can be realized in practice by means of a gray/binary converter [18].

IV. PCTH SIGNAL

In the PCTH scheme, the output of the DSP unit is transformed into an analog signal by means of the D/A converter shown in Fig. 2.¹ A constant offset is then added to this analog signal to form the modulation signal $m(t)$, used to drive the pulse-position modulator.

A. Synchronization Frame

We assume that each pulse is allocated, according to the pseudo-chaotic modulation signal, within a synchronization frame, as shown schematically in Fig. 4. In other words, we assume the existence of a periodic reference, with period T_f , such that only one pulse is transmitted within each frame time T_f (coinciding with the symbol period).² From Fig. 4 we note also that each frame time includes a “guard” time, t_g , (proportional to the offset in the modulation signal) for avoiding overlapping between adjacent pulses. Each pulse can occur at any of $N = 2^M$ discrete time instants, where M is the number of bits in the shift register R . In Fig. 4, the timeslot

¹Note that in case the PPM accepts digital “words” the D/A converter is superfluous.

²This is a standard assumption for the analysis of virtually any communication system. Synchronization can be acquired, for instance, by means of a synchronizing preamble.

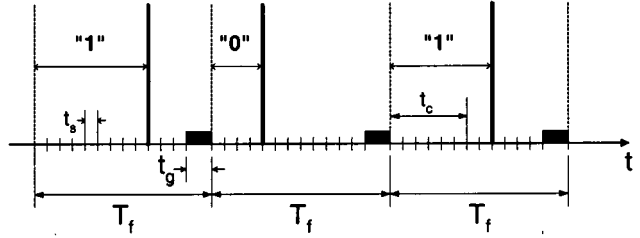


Fig. 4. Sketch of the periodic synchronization frame. Each frame time T_f includes a “guard” interval t_g in order to avoid pulse overlapping. The time delay t_c (with respect to each frame start) corresponds to the partition point $c = 0.5$ of the tent map, and discriminates between the symbols “0” and “1”. The time slot associated with each PPM level is denoted by t_s .

corresponding to each level of the PPM has been denoted by t_s . Note that the value of t_s is limited from below by the system time-base resolution. Also, by neglecting the guard interval t_g , it follows that $t_s \simeq T_f/N$.

We now discuss the encoding of the information according to the symbolic dynamics of the tent map. To this end, we consider the usual partition with respect to the critical point $c = 0.5$, and indicate with t_c the corresponding time delay from the beginning of the frame. Then, by denoting with t_k the relative time (again referred to the beginning of the frame) at which the k -th pulse occurs, if $t_k < t_c$ a “0” is being transmitted, while a “1” is being transmitted if $t_k > t_c$. The situation is illustrated in Fig. 4.

The use of a periodic-synchronization frame enhances the robustness of the scheme in the presence of noise and spurious pulses by preventing error propagation phenomena.³

B. Multilevel PPM

Let’s indicate by $N (= 2^M)$ the number of levels at the transmitter. In PPM M bits are transmitted in each frame time by associating the pulse position with one of the $N = 2^M$ levels. The PCTH scheme utilizes an N-PPM multilevel modulation with input bit “coded” through the chaotic map, with rate $1/M$.

We emphasize that for the proposed scheme the number N_R of levels at the transmitter in general differs from those at the receiver. In particular, the relation $N_R \leq N$ holds. This allows a certain flexibility in the design of the receiver, as discussed in detail in Section V-D.

C. Gaussian Monocycle

In this work it is assumed that each transmitted pulse $w(t)$ has the same shape. A commonly accepted model for the pulse generated by certain types of UWB impulse radio [19] is the so-called *Gaussian monocycle*

$$w(t) = 2\sqrt{e}A\pi t f_c \exp[-2(\pi t f_c)^2] \quad (6)$$

where A determines the peak amplitude of the pulse and f_c determines its center frequency. A normalized plot of $w(t)$ is shown in Fig. 5. Note that expression (6) represents the first derivative of a Gaussian function. This reflects the derivative

³This indeed could be the case when relying on a completely differential scheme, with the information being encoded solely in the inter-pulse time intervals.

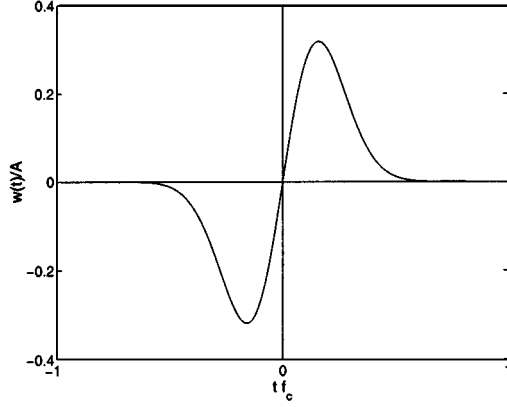


Fig. 5. Plot of the Gaussian monocycle $w(t)$ in normalized units. The pulse duration τ is defined as the time interval between the pulse's maximum and minimum amplitudes.

action of a typical UWB antenna on a Gaussian-like pulse, typically generated with a step-recovery diode. In the frequency domain the Gaussian monocycle can be expressed as

$$W(f) = -\frac{j}{2} \sqrt{\frac{2e}{\pi}} \frac{A}{f_c^2} f \exp \left[-\frac{1}{2} \left(\frac{f}{f_c} \right)^2 \right]. \quad (7)$$

There exists a direct relationship between the pulse's center frequency f_c and its duration τ , the latter being defined as the time interval between the pulse's max and minimum amplitudes (see Fig. 5). In a practical realization, τ can be as low as a few hundreds pico-seconds.

D. PSD of the Signal Transmitted

In this section, we derive an analytical expression for the power-spectral density (PSD) of the PCTH transmitted signal. For the sake of simplicity, but without loss of generality, we assume $t_g = 0$, that is no guard interval is inserted between successive frames, so that the relationship $T_f = N t_s$ holds exactly (see Fig. 4). Also, for convenience we consider here the case $N = 8$.

In Section II-B, it was noted that the relationship between Markov maps and Markov chains [21]. In particular, an eight-state equivalent description of the tent map as a Markov chain is represented in Fig. 6. If we associate to every state, and consequently to every level in the PPM, the signal waveform transmitted $w_i(t)$, ($i = 1, \dots, N$), we obtain a Markov model of the modulation system. This, in turn, can be studied in terms of its spectral properties.

For this analysis, the input binary symbols are considered to be i.i.d. The signals $w_i(t)$ are simply the Gaussian monocycle $w(t)$, given by (6), delayed within the frame time T_f to the appropriate level (see also Fig. 4):

$$w_i(t) = w(t - it_s), \quad i = 0, 1, \dots, (N - 1).$$

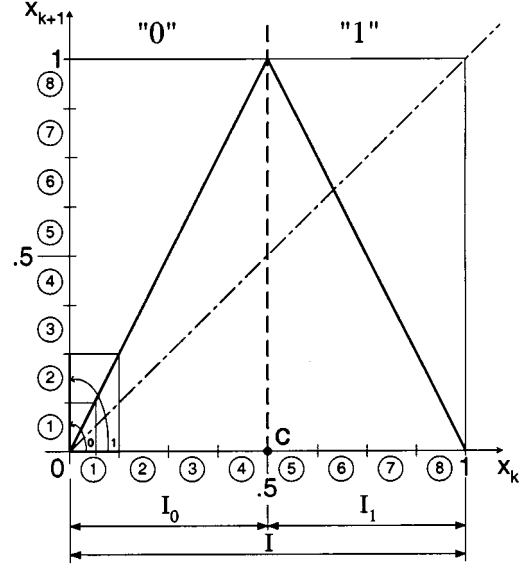


Fig. 6. The tent map with the same definition of the symbolic dynamics as in Fig. 1. Note the Markov partition of the invariant interval I in $N_R (= 8)$ "states" for ML detection purposes. For example, the state 1 (000) can only map to itself or to the state 2 (001), and so on. The transition taking place depends on which half of the subinterval corresponding to the state, the initial value belongs to. The two possible transitions have been labeled by 0 and 1, respectively.

For the Markov chain under consideration ($N = 8$), the matrix P of transition probabilities assumes a quite regular form (see Fig. 10)

$$P = \frac{1}{2} \begin{bmatrix} 1 & 1 & 0 & 0 & 0 & 0 & 0 & 0 \\ 0 & 0 & 1 & 1 & 0 & 0 & 0 & 0 \\ 0 & 0 & 0 & 0 & 1 & 1 & 0 & 0 \\ 0 & 0 & 0 & 0 & 0 & 0 & 1 & 1 \\ 0 & 0 & 0 & 0 & 0 & 0 & 1 & 1 \\ 0 & 0 & 0 & 0 & 1 & 1 & 0 & 0 \\ 0 & 0 & 1 & 1 & 0 & 0 & 0 & 0 \\ 1 & 1 & 0 & 0 & 0 & 0 & 0 & 0 \end{bmatrix}$$

and as the states are equiprobable it follows that: $p_i = p = 1/N$ ($i = 1, \dots, N$), where p_i denotes the stationary probability associated with the i -th state. According to [25], the PSD of the resulting process consists of three terms

$$\begin{aligned} \Phi(f) = & \frac{1}{T_f^2} \sum_{n=-\infty}^{+\infty} \left| \sum_{i=1}^N p_i W_i \left(\frac{n}{T_f} \right) \right|^2 \delta \left(f - \frac{n}{T_f} \right) \\ & \cdot + \frac{1}{T_f} \sum_{i=1}^N p_i |W'_i(f)|^2 + \frac{2}{T_f} \Re \left[\sum_{l=1}^{+\infty} \sum_{i=1}^N \sum_{k=1}^N p_i p_{ik}^{(l)} \right. \\ & \left. \cdot \exp(j2\pi l f T_f) W_i^*(f) W'_j(f) \right] \end{aligned} \quad (8)$$

where

$$w'_i(t) = w_i(t) - \sum_{k=1}^N p_k w_k(t) = w_i(t) - p \sum_{k=1}^N w_k(t)$$

and $W(f)$ is the Fourier transform of the monocycle $w(t)$, given by (7). The elements $p_{ik}^{(l)}$ represent the transition probabilities after l steps or, equivalently, the elements in the matrix P^l .

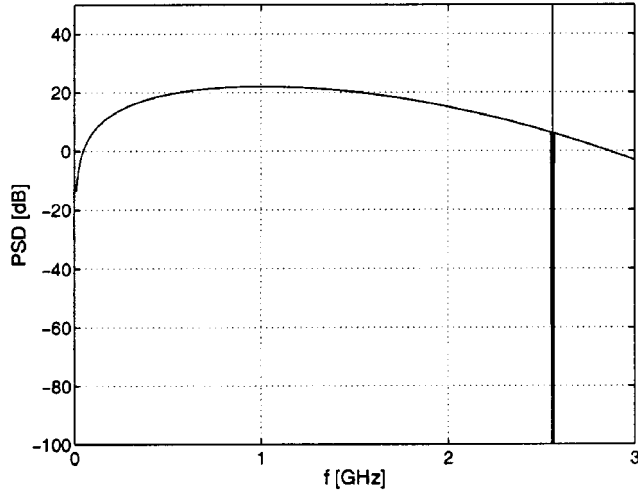


Fig. 7. Analytical estimation of the PSD for the PCTH signal, according to (8), for $1/T_f = 10$ MHz, $N = 256$ levels, and $f_c = 1$ GHz. Note the appearance of the first spectral line at $f_s \simeq 2.56$ GHz.

The first term of (8) is of particular interest because it gives the power of the spectral lines

$$L_n = \frac{1}{T_f^2} \left| \sum_{i=1}^N p_i W_i \left(\frac{n}{T_f} \right) \right|^2.$$

For PPM, L_n can be written as:

$$\begin{aligned} L_n &= \frac{1}{T_f^2} \left| \sum_{i=1}^N p_i W_i \left(\frac{n}{T_f} \right) \right|^2 \\ &= \frac{1}{T_f^2} p \left| W \left(\frac{n}{T_f} \right) \right|^2 \left| \sum_{i=0}^{N-1} \exp(-j2\pi ni/N) \right|^2 \end{aligned} \quad (9)$$

since $T_f = N t_s$, with t_s equal to the time slot assigned to every single level. Also, it is easy to see that

$$\left| \sum_{i=0}^{N-1} \exp(-j2\pi ni/N) \right|^2 = N^2, \quad \text{for } n = 0, N, 2N, \dots$$

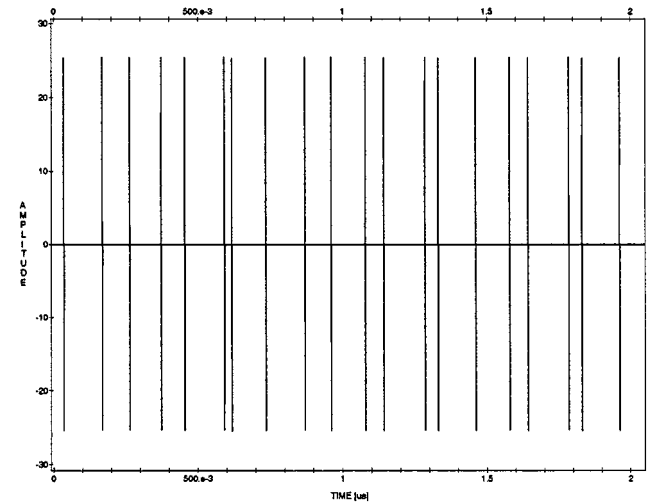
and zero otherwise. This means that the signal (8), without any other constraint on the impulse waveform $w(t)$, has spectral lines at the frequencies which are multiples of the timeslot frequency

$$f_s = 1/t_s = N(1/T_f)$$

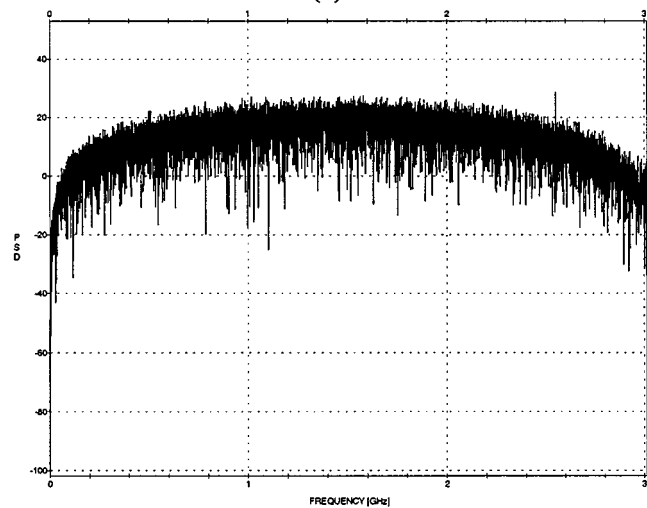
that is 0, $f_s, 2f_s, \dots$, with power decreasing exponentially due to the Gaussian term $W(f)$.

The PSD of the PCTH signal, according to the expression (8) for $N = 256$, is shown in Fig. 7. Note that because of $W(0) = 0$ the line at zero frequency is cancelled. In this example, we chose $T_f = 100$ ns, $M = 8$ bits (resulting in $N = 256$), from which it follows that $t_s \simeq 390$ ps, so that the first spectral line appears at about 2.56 GHz, as visible in Fig. 7. Fig. 8 reports the simulation results for the PCTH transmitted signal obtained with the simulation package SYSTEM VIEW.

Note that in general the spectral lines at frequencies multiples of f_s can be set to fall outside the useful bandwidth, by design.



(a)



(b)

Fig. 8. Simulation results obtained with SYSTEMVIEW. (a) Transmitted PCTH signal with average pulse repetition frequency $1/T_f = 10$ MHz, and $N = 256$ levels. Each pulse is a Gaussian monocycle with center frequency $f_c = 1$ GHz. (b) PSD of the signal transmitted, expressed in decibels.

For a realistic system with $T_f = 100$ ns, $M = 12$ bits, the first spectral line appears at $f_s \simeq 40$ GHz, which is well above the typical UWB range of 1–3 GHz. As a consequence, the resulting spectrum of the PCTH signal can be made featureless, that is very much like noise.

V. PCTH DECODER

This section deals with the detection of the PCTH signal. Note that the PCTH signal is carrier-less (the transmission is baseband) and there is no need to reconstruct a reference signal at the receiver in order to decode the information. As already mentioned, we only assume that the symbol synchronization can be established.

A. Pulse-Position Demodulation

Referring to Fig. 2, the receiver includes a step of pulse-position demodulation (PPD). In the optimal receiver the ideal detection of the incoming pulses is achieved by means of a pulse correlator matched to the pulse shape $w(t)$: this correlator, or

the corresponding matched filter, detects the presence of a transmitted pulse for each position in the time frame. The correlator output provides a measure of the (Euclidean) distance between the received signal and each of the 2^M possible transmitted signals. This measure is then used to feed a soft Viterbi detector in order to perform the optimal detection, at least in AWGN. Alternatively, the correlator output may pass through a decision circuit that estimates the most likely location of the received pulse from the beginning of the frame period: this information is suited to a “hard” implementation of the Viterbi detector (Section VI.C).

B. Threshold Discriminator

In the simplest case the binary information $\tilde{c}(k)$ can be retrieved by means of a threshold discriminator at the output of the PPD. This is shown schematically in Fig. 2. In particular, the decision threshold should be set to the value $c = 0.5$, corresponding to the partition point of the tent map, as shown in Fig. 6.

With the threshold detection described, it is reasonable to expect that critical error events will originate from pulses corresponding to values of the chaotic iterates close to the partition point of the tent map ($c = 0.5$), separating the symbol “0” from the symbol “1”. To reduce this particular error event probability it has been suggested in [26] to create a noise “gap” in the chaotic map around its partition point c . This can be obtained by a proper pre-encoding of the information, forbidding certain sequences of bits. One possibility is to add a line code which avoid series of consecutive zeros. This constraint is usually known as run-length limit constraint and denoted by $RLL(0, k)$, where k indicates the maximum number of allowed consecutive zeros [14].

The capacity of these kinds of line codes is high: for example a code $RLL(0, 3)$ has a capacity equal to 0.9468, while for a code $RLL(0, 4)$ the capacity is 0.9752.⁴ Of course, there is a trade-off between noise resistance and capacity. In particular, in [26] it has been shown that for the case of the logistic map the relationship between the topological entropy h_T ⁵ of the chaotic invariant and the size s (see Fig. 9) of the noise-resisting gap around the partition point follows a descending devil staircase behavior.

C. ML Detection

In general, the optimal receiver for a given transmission system is constituted by a trellis matched to the code and to the expected signals. For each symbol period, the detector should estimate the correlation between the received signal and the N_R expected signals, selecting the sequence with the maximum total correlation according to the code constraint. This is known as ML detection [27] and can be achieved in practice by applying the Viterbi algorithm [16]. Note that the Viterbi algorithm allows the recovery of a part of the received errors and that its correction capability is related to the distance induced by the pseudo-chaotic encoding (Section VI). Some work in the direction of deriving an optimal estimator for a

⁴We recall that the capacity is the maximum achievable rate given the set of constraints realized by the code.

⁵The topological entropy h_T of a chaotic process viewed as information channel may be considered as a measure of the channel capacity [26].

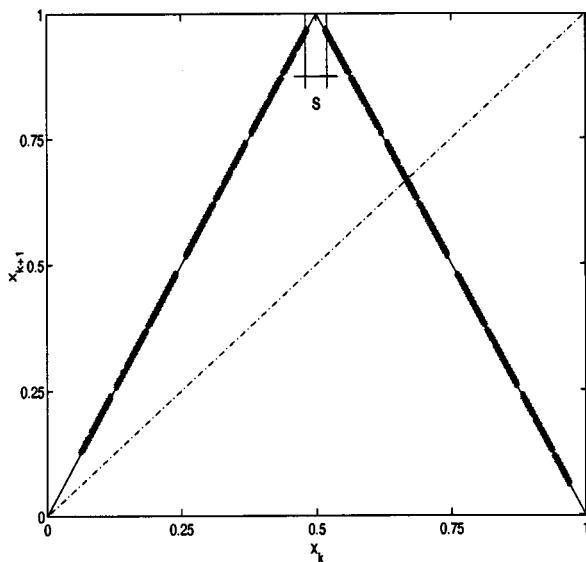


Fig. 9. Numerical simulation of the tent map (generated by the PCTH transmitter) with the line code $RLL(0, 4)$ constraint. Note the creation of a noise “gap” s around the partition point $c = 0.5$.

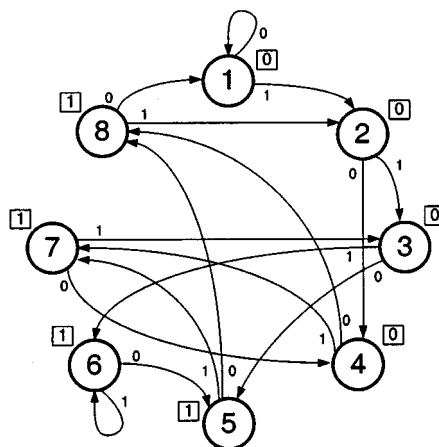


Fig. 10. Equivalent state diagram of the tent map with the state definition of Fig. 6. The transition probabilities equal $1/2$ for every branch. The output values, according to the symbolic dynamics defined on the tent map, are shown (boxed) beside the corresponding state.

chaotic process in additive white gaussian noise (AWGN) has been reported in [28]–[30].

In order to use ML detection for decoding the PCTH signal we consider again the Markov partition of the invariant interval $I = [0, 1]$ of the tent map in $N_R (\leq N)$ symbolic “states”. The situation is illustrated in Fig. 6, for the case $N_R = 8$. The transitions between different states are governed by the dynamics of the map. In particular, only certain transitions (in this case two) are allowed from each state. For instance, referring to Fig. 6, it is clear that the interval corresponding to the state 1 can only map to itself or to the state 2. More precisely, the transition taking place depends on which subinterval associated with the state, the generic iterate x_k belongs to. In Fig. 6 the two possible transitions have been labeled with 0 and 1, respectively. Note that in the case of the tent map, being characterized by a slope in modulus equal to two almost everywhere, the transitions probabilities between states coincide (and equal $1/2$).

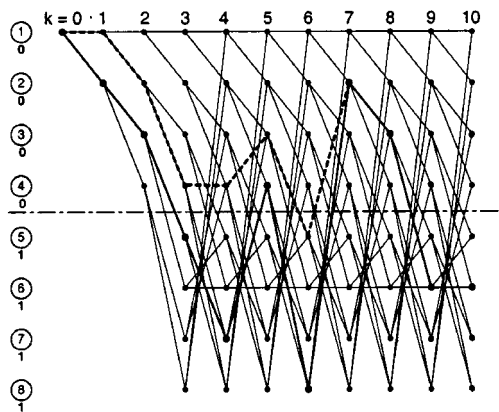


Fig. 11. Trellis associated with the transition diagram in Fig. 10, till $k = 10$. Below each state is indicated the corresponding output. The occurrence of an error event with the wrong path merging with the correct one at $k = 7$ is indicated by a dashed line.

The Markov chain associated with the tent map (with the partition in Fig. 6) can be represented by means of an equivalent state diagram, as illustrated in Fig. 10. The transition branches have been labeled according to the finer partition of the states in subintervals, as shown in Fig. 6. Also, in Fig. 10, we have indicated (within a box) the value of the output corresponding to each state, according to the PCTH encoding of the information. The trellis corresponding to the transition diagram of Fig. 10 is reported in Fig. 11.

D. Receiver Scalability

One of the most interesting features of the PCTH system is the possibility of realizing the Viterbi detector with a number N_R of states lower than the transmitter's one. This can be obtained simply by matching the VD at the receiver to the map with a lower number of symbolic states. Given the transmitter number of states, N , one has a broad range of possibilities for decoding the PCTH signal. Namely, one can choose between VD's with increasing complexity from $N_R = 2, 4, 8, \dots$, till to the full complexity, that is $N_R = N$. This scaling property enables the coexistence of receivers of different complexity (and performance) functioning with the same transmitted signal, which could have some practical implications. In addition, scalability can mitigate the effect of the timing jitter by making the timing requirements at the receiver less stringent than at the transmitter side.

Finally, when a generic chaotic map is implemented by the DSP in the transmitter, the receiver should include a further function after the detector in order to exploit the scalability feature. This additional function reconstructs the transmitted message given the estimated sequence of states provided by the detector itself. This function is an *output mapper* (see Fig. 2), that will be, in general, a finite-state machine (FSM). For particular cases and for appropriate choices of the input/output labels of the encoding map like in the Bernoulli shift and in the tent map, this FSM is not necessary.

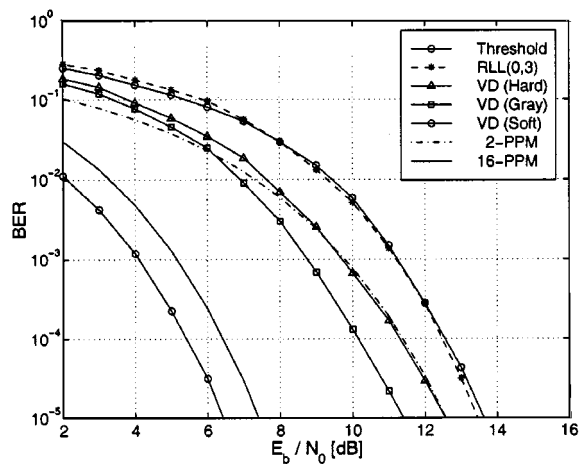


Fig. 12. BER performance of the PCTH scheme in the presence of AWGN. Note that the use of the RLL constraint shows only a slight improvement with respect to the threshold decision, for sufficiently high SNR. On the other hand, ML detection using hard Viterbi decoding exhibits a significant gain. Labeling the states according to the Gray code results in a performance enhancement. Finally, the curve resulting from soft Viterbi decoding and corresponding to the optimal receiver for the PCTH scheme outperforms the previous ones. The simulation results shown have been obtained with $N = N_R = 16$ states. The curves corresponding to ideal 2-PPM and 16-PPM are also plotted for reference purposes.

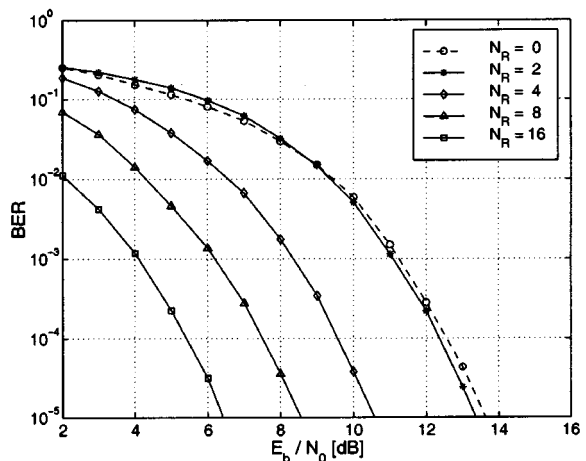


Fig. 13. Scalability of the PCTH receiver with respect to the number N_R of states in the (soft) Viterbi detector. The threshold decision corresponds to the case $N_R = 0$. Note how the BER performance improves when increasing the number of states. Incidentally, for low SNR the case $N_R = 2$ performs slightly worse than the threshold detection; this can be explained because of the limited distance provided by the corresponding trellis for $N_R = 2$.

VI. BER PERFORMANCE

This section reports a bit-error rate (BER) performance analysis of the PCTH scheme for various types of detector. The results of our analysis are presented in terms of BER probability versus the signal-to-noise ratio (SNR) at the receiver, expressed in decibels. The SNR is given by the ratio E_b/N_0 , where E_b is the energy per user bit and N_0 is the single-sided spectral noise density ($\sigma_n^2 = N_0/2$). For the purposes of this analysis we consider the interference on the channel to be just AWGN, that is we neglect nonidealities such as the timing jitter. The latter assumption implies that the time base at the transmitter can be controlled with sufficient accuracy and/or the scalability property plays a mitigation effect on the jitter (see Section V.D).

TABLE I

ERROR EVENT CHARACTERIZATION. THE DOMINANT ERROR EVENTS DEPENDING ON THE NUMBER N_R OF STATES OF THE VITERBI DETECTOR ARE LISTED. WE DENOTE BY d_H THE MINIMUM HAMMING DISTANCE. NOTE THAT THE INPUT ERROR EVENTS ARE REPORTED IN TWO'S COMPLEMENT FORM (FOR INSTANCE 1 CORRESPONDS TO $0 \leftarrow 1$ AND $1 \leftarrow 0$). FOR A DETAILED EXPLANATION REFER TO THE TEXT

No. states	d_H	No. error events	Error event	Length	Input weight
2	1	4	1	2	1
	2	8	11	3	2
	3	16	111	4	3
	4	32	1111	5	4
4	3	8	1	3	1
	4	16	11	4	2
	5	32	111	5	3
8	6	48	1,11	4,5	1,2
	8	64	111	6	3
16	8	64	11	6	2
	10	32	1	5	1

A. Numerical Simulations

The BER performance of the PCTH scheme has been evaluated by means of numerical simulations for the case of $N = 16$ transmitter levels. In Fig. 12 it is visible the curve corresponding to the threshold discriminator, as discussed in Section V-B. Our simulations suggest that the use of the RLL coding (discussed in Section V-B) in conjunction with PCTH offers only a modest improvement, with respect to the threshold decision. On the other hand, Fig. 12 shows that ML detection using a 16-states Viterbi detector with hard metric (Hamming distance) exhibits a significant gain versus the threshold decision. A further performance gain can be achieved by labeling the states according to the Gray code, as confirmed by the corresponding curve in Fig. 12. In addition, Fig. 12 shows the curve resulting from soft Viterbi decoding (Euclidean distance) which clearly outperforms the previous ones. This curve indeed corresponds to the optimal receiver for the PCTH signal.

In order to confirm the scaling properties of the detector, we show in Fig. 13 the simulation results for a receiver based on a soft VD with an increasing number of states. The scalability of the receiver suggests the possibility of a trade-off between the number of transmitter levels, which could translate into a large number of users, and the performance of the receiver.

B. Performance Comparison

Referring to Fig. 12, the coding gain of the PCTH scheme can be appreciated by comparing it to an uncoded PPM modulation with two pulses, at the same user data rate. By assuming that the pulses do not overlap (ideal 2-PPM), this represents an example of 2-orthogonal modulation system. This comparison shows the coding gain of the pseudo-chaotic encoding, even when the type of detection simulated is suboptimal. Note that the curve corresponding to the Gray labeling of the states intersects the ideal 2-PPM curve, showing an appreciable coding gain. Fig. 12 also shows for reference purposes the theoretical BER curve corresponding to 16-PPM. The comparison with PCTH (with $N_R = N = 16$) in this case has to be carried out in terms of spectral efficiency, as 16-PPM is characterized by the same bandwidth occupation as PCTH but higher data rate.

C. Theoretical Performance Bounds

Once fixed the number of states of the Viterbi detector at the receiver it is possible to carry out an analysis of the corresponding trellis in terms of the error event distribution. The characterization of the error events allows a qualitative analysis of the chaotic map as a coding system and a performance estimation, for a given noise statistics and detector implementation.

In this work, we consider the tent map (5) as chaotic map, with $N = 16$ transmitter levels. In Table I a count of the dominant error events for the trellises with 2, 4, 8, 16 states (see the first column), is listed. In the second and sixth column we reported the output Hamming distance and the input error event weight, respectively. It is interesting to note that the minimum Hamming distance, d_H , for each error event increases with the number N_R of states of the VD. On the other hand, the third column of Table I lists the total number of error events found in the trellis, for each state. The trellis under consideration exhibits the same distribution of error events from every state. The structure of the error events observed is quite simple, namely it reduces to successions of the same symbol (e.g., 111...), as illustrated in the fourth column of Table I. We emphasize that, at least for the minimum Hamming distance, the error events are not path sensitive. In other words, the trellis is such that every possible input sequence admits one error event for a given Hamming distance, in a similar fashion to linear codes. Finally, it is worthwhile noting that, up to the distances considered in Table I, the error event lengths (reported in fifth column) and the input weights are always bounded. This indicates that the corresponding trellis do not suffer from catastrophic error propagation.

The optimal receiver for the PCTH scheme consists of a matched filter as PPD, followed by *soft* Viterbi detection. Namely, the PPD computes the Euclidean distance between the received signal and the signal corresponding to each possible pulse position in the frame; this measure is then used to feed a soft Viterbi detector. The Viterbi detector returns the ML sequence of symbols according to the pseudo-chaotic encoding imposed at the transmitter.

For convenience in this analysis we assume the pulses in the channel to be orthogonal, namely they do not overlap. Under

this hypothesis, the probability of confusing each pulse with any other one is given by: $Q(\sqrt{E_B/N_0})$ [14]. Note that the pseudo-chaotic encoding increases the distance between the valid sequences. In fact, each error event defines two paths characterized by two different output sequences. More precisely, because of the specific trellis structure resulting from the pseudo-chaotic encoding, each output coincides with the next state along the path. As in general the two paths (correct and wrong) go through different states as a result of the error event, the coding gain turns out to be the error event length diminished by one, as by definition the two paths merge eventually onto the same state (see Fig. 11). Based on this discussion, the error probability can be bound from above by the following formula:

$$P_{\text{SOFT}} \leq \sum_E N_E \alpha_E Q(\sqrt{E_B \cdot (l_E - 1)/N_0}) \quad (10)$$

where the sum is extended to the dominant error events E . N_E is the input weight associated to the error event E , while l_E denotes its length. The coefficient α_E is given by

$$\alpha_E = \left(\frac{N}{N_R} \right)^{l_E - 1} \quad (11)$$

and takes into account the trellis scalability (see Section V-D). In fact, implementing the receiver with $N_R < N$ ($N =$ transmitter levels) is equivalent to considering only the first $\log_2(N_R)$ MSB bits of every received signal and discarding the others. Therefore, to each state of the reduced trellis correspond N/N_R possible transmitted signals, corresponding to the discarded bits. This infers that the received signal can be confused with other N/N_R signals identifying the concurrent states in the wrong path. Hence, in a trellis path with $(l_E - 1)$ consecutive different symbols, the received signal can be confused with $(N/N_R)^{l_E - 1}$ competing signals for each error event E .

Note that the upper bound (10) is valid under the assumption that the error events are path insensitive, as concluded from the trellis analysis (see Section VI-C). In the general case, though, the error events need to be conditioned to the transmitted sequence.

The optimal receiver can be simplified in several aspects. For instance, instead of computing the Euclidean distances based on the received sequence, an estimation of the pulse position within each frame can be performed, providing an *hard* input to the Viterbi detector. This in turn carries out the detection based upon the Hamming distance among the sequences.

The performance estimation in the suboptimal case utilizes again the knowledge of the dominant error events in the trellis. An upper bound for the error probability should take into account the following terms:

$$P_{\text{HARD}} \leq \sum_E \sum_{k=1}^{l_E - 1} N_E \gamma_E(k) \binom{l_E - 1}{k} p^k (1 - p)^{l_E - 1 - k} \quad (12)$$

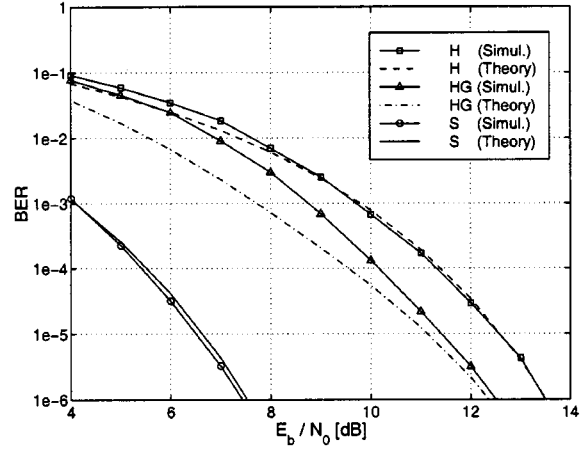


Fig. 14. Simulations versus theoretical performance bounds ($N = N_R = 16$). The simulation results tend to approach the theoretical performance bounds for sufficiently high SNR, in the case of hard (H) and soft (S) Viterbi decoding. On the other hand, for the Gray labeling case (HG) an analytical approximation of the error probability is plotted, according to (13).

where we used the same notations as in (10), and for each error event E

- k number of wrong states out of $(l_E - 1)$ along the wrong path (the last state coincides as the two paths merge at the end of the error event).
- $\gamma_E(k)$ probability that, given E and k , the error count exceeds the threshold given by the Hamming distance guaranteed by E .
- $p = \alpha_E \cdot Q(\sqrt{E_B/N_0})$ probability of a state to be confused with another state belonging to the competing path; for scaled trellises $\alpha_E = N/N_R$ as each state in the reduced trellis maps to N/N_R transmitter levels.

We highlight that, in addition to the metric adopted, the performance of the Viterbi detector depends also on the labeling of the symbolic states defined on the chaotic map. The different labeling affects the factor $\gamma_E(k)$ in (12). For instance, a state ordering according to the Gray code [14] enhances the performance of the system in the presence of noise. An analytical estimation of performance for a different labeling generally requires the expression (12) to be extended to path sensitive error events. For evaluating this case we have to consider the impact of the most important error events on each possible sequence. In fact, depending on the sequence, an error event E generates a distribution P_D of output Hamming distances. In other words, the error event probability depends on the transmitted sequence. For each distance d of the distribution P_D and similarly to (12), we compute $\gamma_E(k)$ given the number k of incorrect steps within the portion of the path interested by E ; now $\gamma_E(k)$ depends also on d . Thus (12) can be generalized as follows:

$$P_{\text{HARD}}^{(\text{Gray})} \leq \sum_E \sum_{d=1}^{d_{\text{max}}} \sum_{k=1}^{l_E - 1} P_D(d) N_E \gamma_E(d, k) \cdot \binom{l_E - 1}{k} p^k (1 - p)^{l_E - 1 - k} \quad (13)$$

In this work, in order to limit the computation, we consider only the error events with smaller Hamming distance, thus obtaining

a performance estimate (rather than a performance bound) for the Gray labeling case.

D. Theory versus Simulations

Fig. 14 shows a comparison of the numerical simulations versus the theoretical performance bounds derived in Section VI.C for soft (S) and hard (H) Viterbi decoding, respectively. We plotted here the curves for high SNR in order to emphasize their asymptotic behavior. As the theoretical curves represent upper bounds, the corresponding simulations are supposed to exhibit a lower error probability. This is confirmed by Fig. 14. The optimal detection using soft Viterbi decoding shows a gain of about 6 dB over the suboptimal hard detection at an error probability of 10^{-4} . As observed in section C.3, a different labeling (e.g., by means of a Gray code) of the states can provide a noticeable enhancement of the hard decoding performance. At 10^{-4} the hard Gray curve (HG) limits the gain loss of about 1 dB. Also, for the latter case we plot in Fig. 14 an approximate analytical estimation of the error probability according to (13), showing a qualitative agreement with the simulation results.

VII. CONCLUSION

In this paper, we have proposed an almost “all-digital” solution suitable for UWB impulse radio systems. The PCTH scheme exploits the symbolic dynamics of a chaotic map for encoding the digital information and multilevel PPM for modulating it into the channel. The pseudo-chaotic modulation has the advantage of producing a noise-like spectrum. This is a desirable feature in terms of LPI and to reduce interference toward other users. The scheme is applicable of ML detection by using the standard Viterbi algorithm. In contrast to conventional convolutional coding, the PCTH decoder is scalable, adding flexibility in terms of the receiver design. For the proposed PCTH scheme we have evaluated the BER performance by means of numerical simulation and derived theoretical performance bounds based on the trellis analysis.

Future work will be directed toward spectral shaping and to extend the application of PCTH to a real multiuser environment.

ACKNOWLEDGMENT

The authors would like to thank Prof. H. Abarbanel, Prof. L. Larson, Prof. K. Yao, Dr. L. Tsimring, Dr. M. Sushchik, Dr. A. Volkovskii, and A. Dati, for the stimulating discussions; and the anonymous reviewers for constructive comments.

REFERENCES

- [1] M. Z. Win and R. A. Scholtz, “Impulse radio: How it works,” *IEEE Commun. Lett.*, vol. 2, pp. 36–38, Feb. 1998.
- [2] S. S. Kolenchery, J. K. Townsend, and J. A. Freebersyter, “A novel impulse radio network for tactical military wireless communications,” in *Proc. MILCOM’98*, Boston, MA, Oct. 18–21, 1998, pp. 59–65.
- [3] R. A. Scholtz, “Multiple access with time hopping impulse modulation,” presented at the *Proc. MILCOM’93*, Bedford, MA, Oct. 11–13, 1993.
- [4] P. A. Bernhardt, “Chaotic frequency modulation,” in *Proc. SPIE*, vol. 2038, 1993, pp. 162–81.
- [5] N. F. Rulkov and A. R. Volkovskii, “Threshold synchronization of chaotic relaxation oscillations,” *Phys. Lett. A*, vol. 179, no. 4–5, pp. 332–336, 1993.
- [6] H. Torikai, T. Saito, and W. Schwarz, “Synchronization via multiplex pulse trains,” *IEEE Trans. Circuits Syst. I*, vol. 46, pp. 1072–1085, Sept. 1999.
- [7] M. Sushchik, N. Rulkov, L. Larson, L. Tsimring, H. Abarbanel, K. Yao, and A. Volkovskii, “Chaotic pulse position modulation: A robust method of communicating with chaos,” *IEEE Commun. Lett.*, vol. 4, pp. 128–130, Apr. 2000.
- [8] T. Yang and L. O. Chua, “Chaotic impulse radio: A novel chaotic secure communication system,” *Int. J. Bifurcation Chaos*, vol. 10, pp. 345–357, Feb. 2000.
- [9] R. G. Aiello, G. D. Rogerson, and P. Enge, “Preliminary assessment of interference between ultra-wideband transmitters and the global positioning system: A cooperative study,” in *Proc. National Technical Meeting of the Institute of Navigation*, Jan. 2000.
- [10] G. M. Maggio, N. Rulkov, M. Sushchik, L. Tsimring, A. Volkovskii, H. Abarbanel, L. Larson, and K. Yao, “Chaotic pulse-position modulation for ultrawide-band communication systems,” in *Proc. UWB’99*, Washington, DC, Sept. 28–30, 1999.
- [11] S. Hayes, C. Grebogi, and E. Ott, “Communicating with chaos,” *Phys. Rev. Lett.*, vol. 70, no. 20, pp. 3031–3034, 1993.
- [12] J. Schweizer and M. P. Kennedy, “Predictive Poincaré control: A control theory for chaotic systems,” *Phys. Rev. E*, vol. 52, no. 5, pp. 4865–4876, 1995.
- [13] B. Hao and W. Zheng, *Applied Symbolic Dynamics and Chaos*. Singapore: World Scientific, 1998.
- [14] J. G. Proakis, *Digital Communications*, 3rd ed. New York: McGraw Hill, 1995.
- [15] E. Ott, *Chaos in Dynamical Systems*. Cambridge, U.K.: Cambridge Univ. Press, 1993.
- [16] G. D. Forney, “The Viterbi algorithm,” *Proc. IEEE*, vol. 61, pp. 268–273, Mar. 1973.
- [17] R. L. Devaney, *A First Course in Chaotic Dynamical Systems*. New York: Addison-Wesley, 1992.
- [18] M. P. Kennedy, “A nonlinear dynamics interpretation of algorithmic A/D conversion,” *Int. J. Bifurcation Chaos*, vol. 5, no. 3, pp. 891–893, 1995.
- [19] H. F. Harmuth, *Nonsinusoidal waves for Radar and Radio Communication*. New York: Academic Press, 1981.
- [20] R. Shaw, “Strange attractors, chaotic behavior and information flow,” *Z. Naturforschung A*, vol. 36A, no. 1, 1981.
- [21] T. Cover and J. Thomas, *Elements of Information Theory*. New York: Wiley, 1991.
- [22] J. P. Cruthfield and K. Young, “Inferring statistical complexity,” *Phys. Rev. Lett.*, vol. 63, no. 2, 1989.
- [23] C. Williams, “Robust chaotic synchronization for communications,” in *Proc. ECCTD’99*, Stresa, Italy, Aug. 29–Sept. 2 1999, pp. 441–44.
- [24] D. Lind and B. Marcus, *An Introduction to Symbolic Dynamics and Coding*. Cambridge, U.K.: Cambridge Univ. Press, 1995.
- [25] P. Galko and S. Pasupathy, “The mean power spectral density of Markov chain driven signals,” *IEEE Trans. Information Theory*, vol. 27, Nov. 1981.
- [26] E. Bollt, Y. C. Lai, and C. Grebogi, “Coding, channel capacity, and noise resistance in communicating with chaos,” *Phys. Rev. Lett.*, vol. 79, no. 19, pp. 3787–3790, 1997.
- [27] R. M. Gagliardi, *Introduction to Communications Engineering*. New York: Wiley, 1988.
- [28] S. Kay and V. Nagesha, “Methods for chaotic signal estimation,” *IEEE Trans. Signal Processing*, vol. 43, pp. 2013–2016, Aug. 1995.
- [29] H. C. Papadopoulos and G. W. Wornell, “Maximum likelihood estimation of a class of chaotic signals,” *IEEE Trans. Commun.*, vol. 46, pp. 881–890, July 1998.
- [30] T. Schimming and J. Schweizer, “Chaos communication from a maximum likelihood perspective,” in *Proc. NDES’99*, Ronne, Denmark, July 15–17, 1999, pp. 179–182.



Gian Mario Maggio (S'95–M'99) received the five-year honors degree and the Ph.D degree, both in electrical engineering, from the Politecnico di Torino, Turin, Italy, and University College Dublin, Dublin, Ireland, in 1995, and 1999, respectively.

In 1995, he worked as an Electronic Designer in the Philips R&D Labs, Milan, Italy. In March 1999, Dr. Maggio joined the Institute for Nonlinear Science (INLS), at the University of California at San Diego (UCSD), La Jolla, as a Post-Doctoral Researcher. Since 2000, he is a Research Engineer

with the Advanced System Technology (AST) group of STMicroelectronics, Inc., San Diego, CA. He is also currently affiliated with the Center for Wireless Communications at UCSD, and acts as the technical liaison AST-UCSD. He held visiting research positions at the Trinity College, Dublin, Ireland, the University of Bristol, Bristol, U. K., the Swiss Federal Institute of Technology, Lausanne, Switzerland, and at the University of California at Berkeley. His main research interests are in the area of nonlinear circuits and systems with applications to wireless communications, iterative-decoding methods and RF oscillators.

He has been the recipient of a Marie Curie fellowship, received the Best Paper Award at the *1999 European Conference on Circuit Theory and Design*. He served as the Track Chair for Nonlinear Circuits and Systems at ISCAS 2001 (Sydney) and is currently the Secretary of the IEEE Technical Committee on Nonlinear Circuits and Systems (TC-NCAS). He serves as a reviewer for a number of conferences and international journals, and organized the Special Session on application of ISCAS 2001 (Sydney), and is the co-organizer of the Winter School on Nonlinear phenomena in Communication networks.



Nikolai F. Rulkov received the M.S. and Ph.D. degrees, both in physics and mathematics, from the University of Nizhny Novgorod, Nizhny Novgorod, Russia, in 1983 and 1991, respectively.

In 1983, he joined the Radio Physics Department of the University of Nizhny Novgorod, where he worked as a Researcher until 1993. He has been with the Institute for Nonlinear Science, University of California, San Diego, from 1993 through the present. His research interests are in the areas of bifurcation theory, nonlinear phenomena, theory of

synchronization, chaos and applications of chaotic oscillations in science and engineering.



Luca Reggiani (S'00) received the honors degree in electronic engineering from the Politecnico di Milano, Milan, Italy, in 1998 and is currently working toward the Ph.D. degree in electronics and communications in the same University.

He has been a visiting scholar at the Center for Magnetic Recording Research, University of California at San Diego, La Jolla, from September 1999 to April 2000. His research interests include coding and detection for magnetic recording systems and information theory.